Two non-proline *cis* peptide bonds may be important for factor XIII function

Manfred S. Weiss[a], Hubert J. Metzner[b], Rolf Hilgenfeld[a,*]

[a] *Institute of Molecular Biotechnology, Department of Structural Biology and Crystallography, P.O. Box 100813, D-07708 Jena, Germany*
[b] *Centeon Pharma GmbH, P.O. Box 1240, D-35002 Marburg, Germany*

Received 8 December 1997; revised version received 23 January 1998

Abstract The structure of recombinant human cellular factor XIII zymogen was solved in its monoclinic crystal form and refined to an *R*-factor of 18.3% (R_{free} = 23.6%) for all data between 40.0 and 2.1 Å resolution. Two non-proline *cis* peptide bonds were detected. One is between Arg^{310} and Tyr^{311} close to the active site cysteine residue (Cys^{314}) and the other is between Gln^{425} and Phe^{426} at the dimerization interface. The structure and the role of these *cis* peptides are discussed in the light of their possible importance for factor XIII function.

Key words: Protein structure; Blood coagulation; Transglutaminase; *cis* Peptide; Factor XIII activation

1. Introduction

Plasma factor XIII (pFXIII) is the last enzyme in the blood coagulation cascade and in contrast to all other enzymes involved, it is not a serine protease but a transglutaminase, catalyzing the formation of isopeptide bonds between the side chains of glutamine and lysine residues. Its main role is to stabilize the fibrin soft clot, and to render it insusceptible to fibrinolysis either by crosslinking of fibrin itself or by crosslinking α_2-antiplasmin, a potent inhibitor of the protease plasmin, onto the fibrin clot [1–3].

Deficiencies in factor XIII can be either acquired or inherited. They inevitably lead to a prolonged coagulation time and to increased occurrence of late bleeding. Furthermore, wound healing disorders have been reported in connection with decreased pFXIII levels [4]. The ability of the enzyme to stabilize blood clots may also have a negative impact. Under certain conditions, the unwanted formation of stabilized clots carries the risk of thrombosis, making it desirable to develop specific factor XIII inhibitors for patients with a high risk of thrombosis.

Factor XIII is found in various tissues and cells. The plasma enzyme exists as an A_2B_2 heterotetramer of a total molecular weight of 320 kDa. A cellular form of factor XIII (cFXIII) has been identified in platelets and monocytes/macrophages. This form exists as a homodimer of two A subunits of 731 amino acids each, with a total molecular weight of 166 kDa.

Activation of factor XIII occurs via proteolysis by the serine protease thrombin in the presence of calcium. Thrombin cleaves a scissile peptide bond between Arg^{37} and Gly^{38}. The activation peptide (residue 1–37) is then thought to dissociate from the protein, thus activating it.

The cellular factor XIII zymogen has been crystallized in two different crystal forms [5] and its structure has been solved in the orthorhombic crystal form (PDB code 1GGT, [6]). Recently, the structure of thrombin-cleaved factor XIII has been reported (PDB code 1FIE, [7]). The enzyme has been described in terms of its domain structure and active site geometry [8]. Both of these structure determinations were at medium resolution (Table 1). We have determined the structure of recombinant cFXIII zymogen at high resolution (2.1 Å) in the monoclinic crystal form and describe some structural details that may be important for the function of the molecule.

2. Materials and methods

Recombinant cFXIII was crystallized following the procedure of Hilgenfeld et al. [5] using the hanging drop technique. 2 μl of protein solution at 2–4 mg/ml were mixed with 2 μl of reservoir solution on a siliconized cover slip and equilibrated against 1 ml of reservoir containing 100 mM MES pH 6.2–6.4 and 1–2% (w/v) PEG-6000. Crystals appeared within one week and continued to grow for a period of two more weeks up to a maximum size of 0.5 mm in each dimension. Sometimes, protein precipitate appeared first and then dissolved again slowly while the crystals were growing.

The crystals were of the monoclinic space group $P2_1$ with unit cell dimensions a = 134.59 Å, b = 72.78 Å, c = 101.05 Å and β = 106.08°. With two molecules of 83 kDa each per asymmetric unit the Matthews parameter [9] was 2.86 Å^3/Da, and the solvent content 57%. The diffraction limit observed was about 2.3 Å using our laboratory source and about 1.9 Å at a synchrotron source.

Crystals were mounted in glass capillaries and subjected to X-ray analysis. Data were collected from two crystals at room temperature on a Nonius FR591 rotating anode generator operated at 40 kV and 100 mA. The CuK_α radiation was monochromatized using a graphite monochromator and the data were recorded on a 30-cm MAR imaging plate. Images were processed using DENZO and scaled using SCALEPACK [10]. Due to the radiation sensitivity of the crystals it was not possible to collect a full dataset from one crystal.

Data from three more crystals were collected at the synchrotron beamline X11 at the EMBL outstation (DESY, Hamburg) at a wavelength of 0.91 Å, also at room temperature. The detector used was a 30-cm MAR imaging plate as well and the data were processed with DENZO and scaled and merged with the data measured in our laboratory using SCALEPACK. Statistics on data collection, processing and scaling are given in Table 2. The data set was of good quality as shown by the overall redundancy of about 3.3 and the conventional merging *R*-factor, as well as by the redundancy-independent merging *R*-factor and the precision-indicating merging *R*-factor [11,12].

The structure was solved using the molecular replacement method implemented in the program XPLOR [13]. The search model was one subunit of the orthorhombic form of factor XIII zymogen (entry 1GGT from the PDB [14], see also Table 1) since at the time the entry 1FIE was not available. For the rotation function data from 15–3.5 Å resolution were used, and a Patterson vector length of 3.5 to 45 Å. From the top ten peaks two solutions that were 180 degrees apart from each other, were identified indicating the orientation of the two molecules in the asymmetric unit. Translation functions in the resolution range 10–3.0 Å yielded highest peaks of 23.6 σ and 15.9 σ

*Corresponding author. Fax: (49) (3641) 656062.
E-mail: hilgenfd@imb-jena.de

PII S0014-5793(98)00098-2

Fig. 1. Overall structure of the factor XIII dimer. The position of the local twofold axis is indicated by (). Within one subunit, the four domains are coloured in yellow, red, green and blue, respectively. The sites of the *cis* peptide bonds are emphasized by *. The figure was produced using the program MOLSCRIPT [28].

for the two molecules. A combined translation function established the relative position of the two molecules with respect to one another. The initial *R*-factor after correctly orienting and positioning the two molecules was 33.8% for all data from 10 to 3.0 Å resolution and it was reduced to 32% after a total of 30 cycles of rigid body refinement. The molecular replacement solution was confirmed using a difference Fourier calculation against a $KAuCl_4$ derivative data set, which showed metal binding sites on Cys^{188} and Cys^{423} of both molecules as the highest peaks.

Model building was carried out with the program O [15] and refinement was done using XPLOR Version 3.1 [13].

After many rounds of manual rebuilding and refinement at gradually increasing resolution, the refinement converged at an *R*-factor of 18.3% (Table 2). All low resolution data to 40.0 Å were included as well as a bulk solvent correction [16] and no amplitude cutoff was applied to the data. Throughout the refinement, non-crystallographic symmetry restraints were maintained for the parts of the structure that are neither involved in nor close to crystal contacts. In order to avoid overfitting of the model, each step of the rebuilding procedure was closely monitored using the free *R*-factor and a residue real space correlation coefficient as a guide.

Accessible surface areas were computed using the program DSSP [17].

Domain-domain interaction free energies were computed based on atomic solvation parameters described by Eisenberg and McLachlan [18]. All the free energy values given are standard-state free energy values.

Sequence searches and comparisons were performed with the GCG program package [19]. The Swissprot protein sequence data base used was release version 34.0 as of November 1996. The search was performed with the program FASTA [20] using the factor XIII sequence 197–503, which constitutes the catalytic or core domain, as the probe.

The coordinates and structure factors, upon which this work is based, have been deposited in the Brookhaven Protein Data Base and will be available under the accession code 1F13.

Table 1
Structural data on FXIII in the PDB [14]

Structure	PDB code	Resolution (Å)	# refs	*R* (%)	R_{free} (%)	Data cutoff [F/σ(F)]
FXIII zymogen [6]	1GGT	10–2.65	65 937	21.6	n.r.[a]	> 2.0
FXIII, thrombin-cleaved [7]	1FIE	10–2.50	49 681	18.2	n.r.	> 2.0

[a]n.r., not reported.

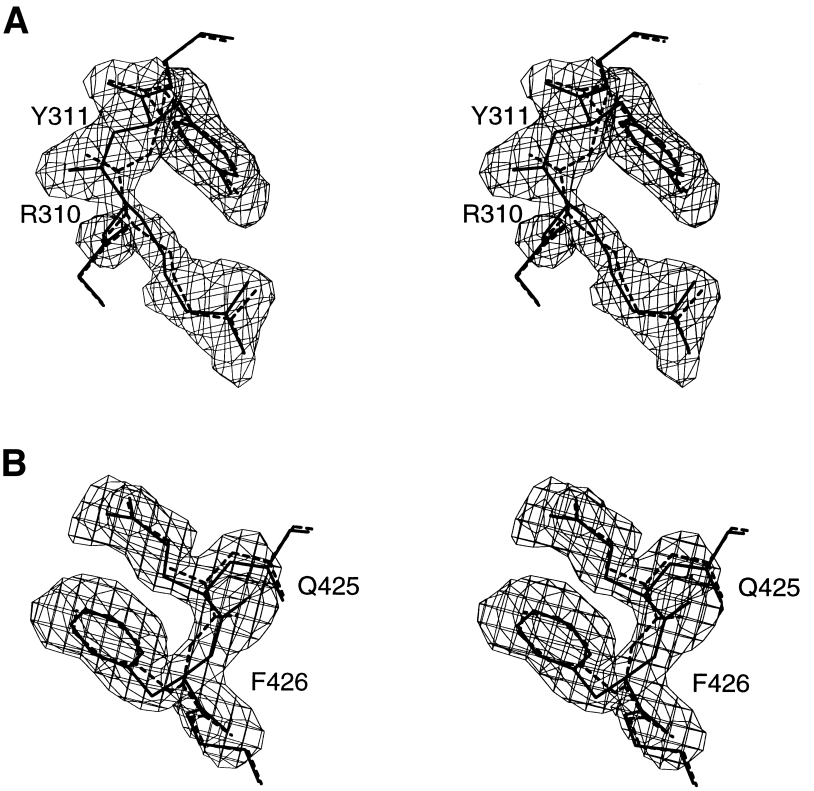

Fig. 2. ($2F_o$-F_c)-electron density of the regions Arg^{310}–Tyr^{311} (A) and Gln^{425}–Phe^{426} (B). The calculated amplitudes and phases for the map are based on a coordinate set that contains *trans* peptide bonds at these sites (shown in dotted lines). The maps are contoured at 1.2 σ (A) and 1.5 σ (B), respectively. The superimposed structures are the model before a *cis* peptide bond was introduced (dotted lines), and the refined model (solid lines). Shown are the sequence stretches 309–312 and 424–427 with only the main-chain atoms for the terminal residues and all atoms for the residues flanking the *cis* peptide bond. Only density around the atoms of the residues 310–311 and 425–426 is displayed. It is clearly evident that the model fits the electron density map better when a *cis* peptide bond is present.

3. Results

Some data on the refinement are summarized in Table 2. The refined structure consists of 11 556 non-hydrogen protein atoms comprising residues 5–36 and 39–728 in subunit 1 and 6–36 and 41–728 in subunit 2, as well as 487 solvent atoms. Almost all of the structure is in well defined electron density except for the terminal residues of the activation peptide and a loop connecting domains 2 and 3. The overall *R*-factor based on all data from 40 to 2.1 Å resolution is indicative of a well refined structure. A Luzzati plot [21] indicated a coordinate error of about 0.25 Å (data not shown).

The structure of the whole dimer is shown in Fig. 1. One subunit consists of four domains, which are colored differently in Fig. 1. The two subunits are related by a proper non-crystallographic twofold axis. For all atoms of the structure, for which non-crystallographic symmetry restraints were kept in the refinement, the r.m.s. deviation between the two molecules is 0.21 Å, which is in the range of the overall coordinate error.

The domain structure of factor XIII has been described previously [6]. Based on secondary structural analysis we delineate the domains in the following way: the activation peptide runs from residues 1 to 37, domain 1 from 38 to 185, domain 2 from 197 to 503, domain 3 from 517 to 628 and domain 4 from 632 to 731. The sequence stretches in between are the connecting loops between the domains. From the structural point of view it might be advantageous to dissect domain 2 into two different domains, one containing just the three-stranded β-sheet seen in the bottom part of Fig. 1. To be consistent with the previous literature we refrained from doing so at that point.

Domain 1 contains almost exclusively β-sheet structure. Two four-stranded β-sheets form an open barrel. In contrast to earlier descriptions, the 37 amino acid long activation peptide does extend this barrel by forming a five residue long β-strand connected to the C-terminal β-strand of the barrel in an antiparallel fashion. A total of 25 direct and at least four water-mediated hydrogen bonds and salt bridges anchor the peptide to the surface of the molecule, its main interactions being to domains 1 and 2 of subunit 1 and domains 2 and 3 of subunit 2 of the dimer. The interaction of the activation peptide with the dimer buries a total of 3700 $Å^2$ of surface on the peptide and on both subunits. The total interaction energy between the activation peptide and the rest of the dimer based on atomic solvation parameters is approximately −14 kcal/mol. From these about −9 kcal/mol account for interactions with subunit 1 and the rest for interactions with subunit 2.

Domains 3 and 4 are both of the fibronectin III type. They contain seven β-strands and are topologically identical. Both domains interact closely with domain 2. In the interaction of domain 2 with domain 3 a total surface area of 3000 $Å^2$ is buried; between domains 2 and 4 this value is 1900 $Å^2$, and between domains 3 and 4 it is 600 $Å^2$. Energetically, the interaction between domains 2 and 3 yields about −11 kcal/mol of free energy, the one between domains 2 and 4 about −3

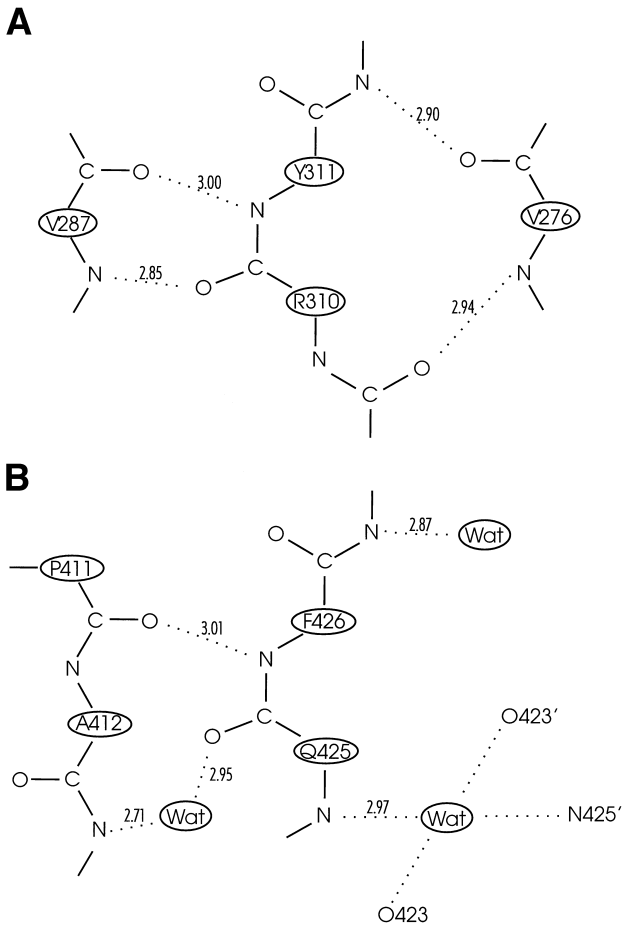

Fig. 3. Schematic representation of the main-chain interactions of the segments Arg^{310}–Tyr^{311} (A) and Gln^{425}–Phe^{426} (B). The distances are measured from subunit 1 atoms and are given in Å. In (B) atoms of the second subunit are marked by ′.

kcal/mol and the one between domains 3 and 4 about −5 kcal/mol.

Domain 2 consists of a central six-stranded β-sheet, a second β-sheet of three strands, a long β-hairpin and a total of nine α-helical segments. The longest α-helix of 17 residues in the center of the molecule contains the active site cysteine, Cys^{314}. The other two members of the catalytic triad, His^{373} and Asp^{396}, are located on adjacent strands of the central six-stranded β-sheet. During the course of the refinement it became evident that two of the peptide bonds in this domain (Arg^{310}–Tyr^{311} and Gln^{425}–Phe^{426}) had to be rebuilt in the *cis* conformation. Locally we observed rather large deviations from ideal geometry and in a (F_o-F_c) difference Fourier synthesis, difference density appeared next to the main chain atoms. As shown in Fig. 2, it is clearly evident that a *cis* peptide bond fitted better to the ($2F_o$-F_c) density than a *trans* peptide bond. The interpretation was also confirmed by an increase in the real space correlation coefficient for the flanking residues upon modelling the *cis* conformation.

The sites of these non-proline *cis* peptide bonds in the structure are in the loop before the central helix that contains the active site Cys^{314} at its N-terminus, and in a loop between two α-helices close to the dimerization interface. Geometrically there seems to be no obvious need for a *cis* peptide bond at these sites as for instance a sharp change in chain direction might require. Also, none of the residues flanking the *cis* peptide are outliers with respect to their main chain dihedral angles. As a matter of fact, all of them are in the β-region of the Ramachandran plot [22].

Stabilization for the energetically unfavoured *cis* conformation comes from two different sources, hydrogen bonding and hydrophobic side-chain interactions. As depicted in Fig. 3A, Val^{287} forms hydrogen bonds with Tyr^{311}-N as well as with Arg^{310}-O. The neighboring residues Val^{309} and Gly^{312} form hydrogen bonds with Val^{276}. Tyr^{311}-O forms a hydrogen bond with the indole nitrogen of Trp^{292}, and Arg^{310}-N is hydrated. If a *trans* peptide bond was modelled, there would be no hydrogen bond donor in close enough proximity to be a partner for Arg^{310}-O. The second source of stabilization is evident from Fig. 2A. The hydrophobic part of the side chain of Arg^{310}, namely C_β and C_γ, packs against the aromatic ring of Tyr^{311} at a distance of less than 3.5 Å, which is too short for a simple van der Waals interaction.

A similar situation was observed for the *cis* peptide bond between Gln^{425} and Phe^{426}. Gln^{425}-O forms a water-mediated hydrogen bond with Ser^{413}-N (Fig. 3B) and Phe^{426}-N is hydrogen bonded to Pro^{411}-O. Pro^{411} is itself involved in a *cis* peptide bond with Gly^{410}. Gln^{425}-N is hydrated by a water

Table 2
Data collection and refinement statistics

Data collection	
Number of crystals	5
Resolution limits (Å)	100–2.1
Total number of reflections	293 385
Unique reflections	89 672
Completeness (%)	81.6
R_{merge} (%)[a]	10.3
$R_{r.i.m.}$ (%)[b]	12.0
$R_{p.i.m.}$ (%)[c]	5.9
Refinement	
Resolution limits (Å)	40–2.1
Data cutoff [F/σ(F)]	0.0
Number of reflections	89 649
Working set	87 854
Test set	1795
R (%)[d]	18.3
R_{free} (%)	23.6
# Protein atoms	11 556
# Solvent atoms	487
Average B-factor (Å^2)	39.7
R.m.s.d. bonds (Å)	0.010
R.m.s.d. angles (°)	1.562

[a] $R_{merge} = \sum_{hkl}\sum_i |I_i(hkl) - \overline{I(hkl)}| / \sum_{hkl}\sum_i I_i(hkl)$, where (hkl) denotes the sum over all reflections and (i) the sum over all equivalent and symmetry-related reflections [29].

[b] $R_{r.i.m.}$ is the redundancy-independent merging R-factor [11].

$$R_{r.i.m.} = \sum_{hkl}\sqrt{\frac{N}{N-1}}\sum_i |I_i(hkl) - \overline{I(hkl)}| / \sum_{hkl}\sum_i I_i(hkl)$$

with N being the number of times a given reflection has been observed.

[c] $R_{p.i.m.}$ is the precision-indicating merging R-factor [11].

$$R_{p.i.m.} = \sum_{hkl}\sqrt{\frac{1}{N-1}}\sum_i |I_i(hkl) - \overline{I(hkl)}| / \sum_{hkl}\sum_i I_i(hkl).$$

[d] $R = \Sigma_{hkl} |F_{obs} - k \cdot F_{calc}| / \Sigma_{hkl} F_{obs}$.

Sequence	Code	% identity	# Amino acids	Region 1	Region 2
Human F13	f13a_human	100.0	307	302 YRSSE.NPV[RY]GQCWVFAG	416 AIKHGHVCF[QF]DAPFVFAEV
Rabbit TGK	tglk_rabit	53.5	303	385 YLRTG.YSV[PY]GQCWVFAG	499 SVKNGLVYM[KY]DTPFIFAEV
Rat TGK	tglk_rat	54.5	303	373 YLRTG.YSV[PY]GQCWVFAG	487 SIKNGLVYM[KY]DTPFIFAEV
Human TGK	tglk_human	54.1	303	365 YLRTG.YSV[PY]GQCWVFAG	479 SIKNGLVYM[KY]DTPFIFAEV
Crab TG	tglh_tactr	49.2	303	330 YLKTRGVPV[KY]GQCWVFAG	445 AVQRGEIGY[MF]DSPFVFSEV
Bream TGC	tglc_pagma	48.0	304	259 WSKAGVRPV[KY]GQCWVFAA	375 AIKEGNLGV[KY]DAPFVFAEV
Grasshopper TG	annu_scham	46.4	304	329 FYKNK.KPV[KY]GQCWVFAG	447 AVKQGEVLR[PY]DSAYVFAEV
Rat TGD	tgld_rat	45.6	305	243 HYITR.MPV[RF]GQCWVFSG	357 AIRQGLVQF[MY]DTTFVFTEV
Human TG4	tgl4_human	43.1	306	256 YYNTK.QAV[CF]GQCWVFAG	365 AIRKGDIFI[VY]DTRFVFSEV
Mouse TGC	tglc_mouse	49.8	309	264 WKEHGCQQV[KY]GQCWVFAA	378 AIKEGDLST[KY]DAPFVFAEV
Human TGC	tglc_human	50.6	310	264 WKNHGCQRV[KY]GQCWVFAA	378 AIKEGDLST[KY]DAPFVFAEV
Bovine TGC	tglc_bovin	49.5	309	264 WKRDGCQRV[KY]GQCWVFAA	378 AIKEGDLST[KY]DAPFVFAEV
Chicken TGC	tglc_chick	50.3	306	273 WKDYGCQRV[KY]GQCWVFAA	387 AIKEGHLNV[KY]DAPFVFAEV
Guinea pig TGC	tglc_cavcu	50.0	306	263 WKDYGCQRV[KY]GQCWVFAA	377 AIKEGHLNV[KY]DAPFVFAEV
Human TG3	tgl3_human	47.9	311	260 WKKSGFSPV[RY]GQCWVFAG	374 GVREGDVQL[NF]DMPFIFAEV
Mouse TG3	tgl3_mouse	47.3	311	260 WKKSGFRPV[QF]GQCWVFAG	374 AIKAGDVDR[NF]DMIFIFAEV
Human P4.2	42_human	33.3	300	254 WLTGRGRPV[YD]GQAWVLAA	369 AVKEGTVGL[TP]AVSDLFAAI
Mouse P4.2	42_mouse	33.7	300	254 WLTGQGRAV[YE]TQAWVSAA	369 AVKEGELQL[DP]AVPELFAAV

Fig. 4. Sequence alignment of human factor XIII with representative transglutaminases in the regions of the *cis* peptide bonds. The code given is the SWISSPROT database code, and the identity is with respect to the alignment against factor XIII. The number of amino acids denotes the total length of the aligned region. The residues directly flanking the *cis* peptide bonds are inside the boxes.

molecule located on the local twofold rotation axis, connecting the two Gln^{425} residues in the dimer. With a *trans* peptide bond present there would be no hydrogen bonding partner for Phe^{426}-O. Also in this case, side chain stacking is observed. The hydrophobic part of the glutamine side chain (C_β and C_γ) packs against the aromatic ring of Phe^{426} at a distance of less than 3.7 Å (see also Fig. 2B).

A sequence alignment between the factor XIII domain 2 sequence and several transglutaminase enzymes from the Swissprot database is presented in Fig. 4. The overall sequence identity in this about 300 amino acid-long stretch ranges between 33 and 55%. The regions of the two *cis* peptide bonds, shown in Fig. 4, exhibit a high degree of sequence conservation. In region 1 all amino acids observed on the N-terminal side of the *cis* peptide bond are either charged or polar residues with long side chains except for a Cys in human transglutaminase 4 and the aromatic residues in the homologous erythrozyte membrane protein band 4.2 (P4.2). On the C-terminal side, only aromatic residues are observed except for the P4.2 proteins, where the aromatic residue has been replaced by negatively charged residues, but instead aromatic residues occur here on the N-terminal side. The region C-terminal to the *cis* peptide bond in region 1 is the active site region, which explains the absolute conservation of these residues. In region 2 as well an almost complete conservation of aromatic residues on the C-terminal side of the *cis* peptide bond can be observed except for the P4.2 proteins which contain proline residues at this site. On the N-terminal side again mostly long polar side chains are observed although slightly less pronounced than in region 1. Furthermore, the Gly^{410}–Pro^{411} *cis* peptide bond seems to be conserved as well, as shown by the absolute conservation of the sequence GlyPro at this site in all transglutaminases. In the P4.2 proteins the proline is shifted two residues towards the C-terminus in the alignment (data not shown). These observations corroborate the notion that *cis* peptide bonds do also occur in all other transglutaminases at these sites and in the P4.2 proteins as well.

4. Discussion

The major problem in understanding the function of factor XIII to date is the activation process. The identified catalytic centre comprising residues Cys^{314}, His^{373} and Asp^{396} is completely buried and therefore unaccessible to the substrate. The activation process includes the cleavage of the scissile peptide bond between Arg^{37} and Gly^{38}, but that alone is not sufficient to expose the active site as was seen in the structural analysis of thrombin-cleaved factor XIIIa′ [7]. The activation peptide did not dissociate spontaneously from the rest of the protein, which in retrospect is not surprising considering the estimated interaction energy of about −14 kcal/mol and a total buried surface area of 3700 $Å^2$.

Even after the hypothetical removal of the activation peptide the active site is still practically unaccessible. In order to expose the active site, domains 2 and 3 need to be separated from each other. This would leave the active site at least partially accessible, which may be enough for catalysis to occur. The problem is, however, how a tight interaction such as the one between domains 2 and 3 (−11 kcal/mol or 3000 $Å^2$ buried surface area) can be broken. The extent of this interaction compares with the one found at the interface of stable oligomeric proteins. According to Janin et al. [23], in a stable oligomer a minimum buried surface of 1200 $Å^2$ is required to overcome the entropy loss upon association. It has been speculated that binding of factor XIII to either the fibrin substrate or some other effector, possibly calcium, could trigger the conformational rearrangement necessary for exposing the active site.

In the X-ray structure of the enzyme in the presence of calcium [24], a binding site for the metal ion has been detected, but no structural changes other than small local rearrangements of the calcium-binding amino acids were observed. Based on this evidence we conclude that calcium ions alone cannot be responsible for the activation process to occur.

Another possible explanation is that binding to the sub-

strate fibrin will cause the active site to become exposed. However, if the energy necessary to break the interaction between domains 2 and 3 is provided by the binding of fibrin, then one tight interaction will be replaced by another and the dissociation problem will just be shifted one step down the line. Moreover, factor XIII is also activated by small substrates like peptides [25], binding of which will not provide such large energies. This underlines the importance of a mechanism of activation that is more independent of binding to substrate than has been previously suggested.

Based on our results, we propose that the protein has an inherent ability to assume two conformational states, and that a *cis*/*trans* isomerization of the peptide bonds Arg^{310}–Tyr^{311}, Gln^{425}–Phe^{426} and Gly^{410}–Pro^{411} may act as a conformational switch between these two states. If one or all of the bonds isomerize to the energetically favored *trans* conformation, local strain along the chain will build up. This could be the trigger for a conformational rearrangement, which leads to a reduction of the binding energy between domains 2 and 3 or even in a partial separation of the two. The remaining energy necessary for exposing the active site could then be provided by substrate binding.

The fact that non-proline *cis* peptide bonds are very rare in protein structures [26] and that the ones described here are found in such peculiar locations (one close to the active site and the other at the dimerization interface in a cluster with a second *cis* peptide bond) strongly suggests a functional role for them. Furthermore, the *cis* peptide bonds are likely to be conserved within the family of transglutaminases, which supports this hypothesis.

Site-directed mutagenesis of either Arg^{310} or Tyr^{311} to Ala [27] reduced the enzymatic activity dramatically, without reducing the binding to fibrin. Especially the Y311A mutation yielded an enzyme without any detectable activity. This also supports our hypothesis of ascribing functional importance to these residues. To our knowledge there have been no point mutations in the region of the second *cis* peptide bond described so far, but we predict that mutating either Gln^{425} or Phe^{426} will affect the function of factor XIII in a similar fashion.

In summary, we have presented a well-refined structure of cFXIII at high resolution, we have discovered two non-proline *cis* peptide bonds in peculiar locations, and we have presented a plausible mechanism of factor XIII activation, which involves the *cis*/*trans* isomerization of the non-proline *cis* peptide bonds. We will continue to investigate this mechanism by crystallographic and other means.

Acknowledgements: We would like to thank Silke Schulz for her help with the crystallization experiments and the staff of the EMBL outstation Hamburg for their kind support and coffee during data collection.

References

[1] Muszbek, L., Ádány, R. and Mikkola, H. (1996) Crit. Rev. Clin. Lab. Sci. 33, 357–421.
[2] Uchino, R., Cardinal, M. and Chung, S.I. (1991) Fibrinolysis 5, 93–98.
[3] Sakata, Y. and Aoki, N. (1980) J. Clin. Invest. 65, 290–297.
[4] Seitz, R., Duckert, F., Lopaciuk, S., Muszbek, L., Rodeghiero, F. and Seligsohn, U. (1996) Semin. Thromb. Hemost. 22, 415–425.
[5] Hilgenfeld, R., Liesum, A., Storm, R., Metzner, H.J. and Karges, H.E. (1990) FEBS Lett. 265, 110–112.
[6] Yee, V.C., Pedersen, L.C., Le Trong, I., Bishop, P.D., Stenkamp, R.E. and Teller, D.C. (1994) Proc. Natl. Acad. Sci. USA 91, 7296–7300.
[7] Yee, V.C., Pedersen, L.C., Bishop, P.D., Stenkamp, R.E. and Teller, D.C. (1995) Thromb. Res. 78, 389–397.
[8] Pedersen, L.C., Yee, V.C., Bishop, P.D., Le Trong, I., Teller, D.C. and Stenkamp, R.E. (1994) Prot. Sci. 3, 1131–1135.
[9] Matthews, B.W. (1968) J. Mol. Biol. 33, 491–497.
[10] Otwinowski, Z. (1993) Oscillation Data Reduction Program. Proceedings of the CCP4 Study Weekend: 'Data Collection and Processing', 29–30 January 1993 (Sawyer, L., Isaacs, N. and Bailey, S., Eds.), pp. 56–62. SERC Daresbury Laboratory, UK.
[11] Weiss, M.S. and Hilgenfeld, R. (1997) J. Appl. Cryst. 30, 203–205.
[12] Diederichs, K. and Karplus, P.A. (1997) Nature Struct. Biol. 4, 269–275.
[13] Brünger, A.T., Kuriyan, J. and Karplus, M. (1987) Science 235, 458–460.
[14] Bernstein, F.C., Koetzle, T.F., Williams, G.J.B., Meyer, E.F., Brice, M.D., Rodgers, J.R., Kennard, O., Shimanouchi, T. and Tasumi, M. (1977) J. Mol. Biol. 112, 535–542.
[15] Jones, T.A., Zou, J.Y., Cowan, S.W. and Kjeldgaard, M. (1991) Acta Cryst. A47, 110–119.
[16] Kostrewa, D. (1997) CCP4 Newsletter 34, 9–22.
[17] Kabsch, W. and Sander, C. (1983) Biopolymers 22, 2577–2637.
[18] Eisenberg, D. and McLachlan, A. (1986) Nature 319, 199–203.
[19] Devereux, J., Haeberli, P. and Smithies, O. (1984) Nucleic Acids Res. 12, 387–395.
[20] Pearson, W.R. and Lipman, D.J. (1988) Proc. Natl. Acad. Sci. USA 85, 2444–2448.
[21] Luzzati, V. (1952) Acta Cryst. 5, 802–810.
[22] Ramachandran, G.N. and Sasisekharan, V. (1968) Adv. Prot. Chem. 23, 283–437.
[23] Janin, J., Miller, S. and Chothia, C. (1988) J. Mol. Biol. 204, 155–164.
[24] Yee, V.C., Le Trong, I., Bishop, P.D., Pedersen, L.C., Stenkamp, R.E. and Teller, D.C. (1996) Semin. Thromb. Hemost. 22, 377–384.
[25] Gorman, J.J. and Folk, J.E. (1981) J. Biol. Chem. 256, 2712–2715.
[26] Stewart, D.E., Sarkar, A. and Wampler, J.E. (1990) J. Mol. Biol. 214, 253–260.
[27] Hettasch, J.M. and Greenberg, C.S. (1994) J. Biol. Chem. 269, 28309–28313.
[28] Kraulis, P.J. (1991) J. Appl. Cryst. 24, 946–950.
[29] Stout, G.H. and Jensen, L.H. (1968) X-ray Structure Determination. A Practical Guide, p. 402, Macmillan Publishing Co., Inc.